Monthly Notices of the ROYAL ASTRONOMICAL SOCIETY
MNRAS **455,** 3393–3404 (2016) doi:10.1093/mnras/stv2491

Envelope overshooting in low-metallicity intermediate- and high-mass stars: a test with the Sagittarius dwarf irregular galaxy

Jing Tang,[1★] Alessandro Bressan,[1★] Alessandra Slemer,[2] Paola Marigo,[2] Leo Girardi,[3] Luciana Bianchi,[4] Phil Rosenfield[2] and Yazan Momany[3]

[1]*SISSA, via Bonomea 265, I-34136 Trieste, Italy*
[2]*Dipartimento di Fisica e Astronomia, Vicolo dell'Osservatorio 4, I-37122 Padova, Italy*
[3]*OAPD, Vicolo dell'Osservatorio 5, I-37122 Padova, Italy*
[4]*Department of Physics and Astronomy, Johns Hopkins University, 407 Bloomberg Center, 3400 N. Charles St, Baltimore, MD 21218, USA*

Accepted 2015 October 22. Received 2015 October 16; in original form 2015 August 20

ABSTRACT

We check the performance of the Padova TRieste Stellar Evolution Code (PARSEC) tracks in reproducing the blue loops of intermediate age and young stellar populations at very low metallicity. We compute new evolutionary PARSEC tracks of intermediate- and high-mass stars from 2 to 350 $M_{\odot}$ with enhanced envelope overshooting (EO), EO = $2H_P$ and $4H_P$, for very low metallicity, $Z = 0.0005$. The input physics, including the mass-loss rate, has been described in PARSEC, version V1.2. By comparing the synthetic colour–magnitude diagrams (CMDs) obtained from the different sets of models with EO = $0.7H_P$ (the standard PARSEC tracks), $2H_P$ and $4H_P$, with deep observations of the Sagittarius dwarf irregular galaxy (SagDIG), we find that the overshooting scale EO = $2H_P$ best reproduces the observed loops. This result is consistent with that obtained by Tang et al. for Z in the range 0.001–0.004. We also discuss the dependence of the blue loop extension on the adopted instability criterion. Contrary to what has been stated in the literature, we find that the Schwarzschild criterion, instead of the Ledoux criterion, favours the development of blue loops. Other factors that could affect the CMD comparisons, such as differential internal extinction or the presence of binary systems, are found to have negligible effects on the results. Thus, we confirm that, in the presence of core overshooting during the H-burning phase, a large EO is needed to reproduce the main features of the central He-burning phase of intermediate- and high-mass stars.

Key words: stars: evolution – Hertzsprung–Russell and colour–magnitude diagrams – stars: interiors – stars: massive.

1 INTRODUCTION

We have updated the new evolutionary tracks of massive stars from 14 to 350 $M_{\odot}$ in Tang et al. (2014). Thus, we have built a complete library of evolutionary tracks from very low ($M = 0.1$ $M_{\odot}$) to very massive ($M = 350$ $M_{\odot}$) stars, from the pre-main sequence to the beginning of central carbon burning. These tracks are computed with the Padova Trieste stellar evolution code (PARSEC). All the input physics, including the mass-loss rate, has been detailed in Bressan et al. (2012, 2013), Chen et al. (2014) and Tang et al. (2014). In this paper, we present the evolutionary tracks of intermediate- and high-mass stars at very low metallicity, $Z = 0.0005$, and test them against the observations of the Sagittarius dwarf irregular galaxy (SagDIG).

Convection plays a crucial role in stellar structure and evolution, but it has not yet been fully understood. Convection is the macroscopic motions with energy and chemical element transport in the stellar interior. The most widely used theory for convection is the mixing length theory (MLT), proposed by Böhm-Vitense (1958). The mixing length parameter is calibrated to be $\alpha_{MLT} = 1.74$ based on the solar model (Bressan et al. 2012). In the MLT, the convective boundary is the location where the acceleration of the fluid elements is zero ($a = 0$). However, at this border, the elements still have a non-negligible velocity. They are able to cross the boundary and enter the stable radiative region until the velocity is zero ($v = 0$). The region lies between $a = 0$ and $v = 0$ is called the overshooting. Bressan, Chiosi & Bertelli (1981) provided a simple way to calculate the overshooting.

As we know, convection occurs not only in the central core but also in the external envelope. Correspondingly, the extension of convective boundary is described by core overshooting above the

★E-mail: tang@sissa.it (JT); sbressan@sissa.it (AB)

Published by Oxford University Press on behalf of the Royal Astronomical Society

convective core and envelope overshooting (EO) at the base of the convective envelope. Much theoretical and observational work supports the existence of core overshooting (Bressan et al. 1981; Bertelli, Bressan & Chiosi 1985; Bertelli et al. 1990). The main parameter describing core overshooting is the mean free path of convective elements across the border of the unstable region, $l_c = \Lambda_c H_P$, where H_P is the local pressure scaleheight. In this work, $\Lambda_c = 0.5$ is adopted (Girardi, Rubele & Kerber 2009), which corresponds to $0.25H_P$ above the unstable region. The consideration of EO in stellar models was first suggested by Alongi et al. (1991). There are two relevant observational constraints: the location of the red giant branch (RGB) bump in globular clusters and old open clusters, and the extension of blue loops in intermediate- and high-mass stars. Both features can be reproduced better by considering a moderate amount of $\mathrm{EO} = 0.7H_P$ (Alongi et al. 1991).

However, Tang et al. (2014) found that a larger mixing scale, $\mathrm{EO} = 2H_P$ or $4H_P$, is preferred to reproduce the extension of the observed blue loops in nearby star-forming dwarf galaxies. This result implies a strong dependence of the mixing scale below the formal Schwarzschild border of the envelope, on the stellar mass or luminosity. In this paper, we calibrate the EO parameter by comparing the synthetic and observed colour–magnitude diagrams (CMDs) of SagDIG, and we further confirm this result.

The presence of blue loops during central He-burning phase was first thoroughly investigated by Lauterborn, Refsdal & Weigert (1971), who introduced the core potential $\phi = M_{\rm core}/R_{\rm core}$ to explain the occurrence. However, many studies show that the proximity of the H-burning shell to the H–He discontinuity, marked by the depth of first dredge up, triggers the blue loop (Lauterborn et al. 1971; Robertson 1972; Stothers & Chin 1991). Thus, any factor that moves the discontinuity deeper into the star causes a more extended loop. This conclusion is supported by Tang et al. (2014) who realized it by enhancing the EO. Further, Walmswell, Tout & Eldridge (2015) demonstrated that this phenomenon is essentially due to the removal of the excess helium above the burning shell, which causes changes to the mean molecular weight as well as the local opacity and the shell fuel supply. They believed that if this happens faster than the core evolution, then the blue loop is triggered.

SagDIG is an ideal candidate to test our models at extremely low metallicity, because it is a very metal-poor star-forming galaxy in the Local Group, and also it is nearby (≈1.1 Mpc), which enables the *Hubble Space Telescope* (*HST*) to resolve its star content well. In Section 2, we briefly describe the photometric data and the observed CMD from which the foreground contamination has been deducted. In Section 3, we discuss the dependence of the blue loop extension on the adopted convection criterion, and present the new evolutionary tracks of intermediate- and high-mass stars computed by PARSEC with different EO. In Section 4, we review the technique used to construct the synthetic CMDs, and in Section 5, we show the comparison of different models with the observed CMD of SagDIG. Finally, we discuss and conclude in Section 6.

2 DATA

2.1 Colour–magnitude diagram

To test our models, we use deep observations of SagDIG with the Advanced Camera for Surveys (ACS) on board the *HST*. The observations contain two-epoch data sets (GO-9820 and GO-10472) that are separated by ~2 yr. The main body of the galaxy ($l = 21\overset{\circ}{.}06$, $b = -16\overset{\circ}{.}28$) was imaged in three filters: F475W, F606W and F814W. More details on the observations and data reduction can be found in Momany et al. (2014).

Because of its low latitude, SagDIG suffers a heavy Galactic contamination but Momany et al. (2014) used data from two epochs to analyse the relative proper motions of all detected stars and to correct for foreground contamination. The CMDs cleaned for such a contamination of SagDIG are shown in Fig. 1, for filters F475W and F606W and for filters F606W and F814W, in the left and right panels, respectively.

The high-resolution *HST*/ACS observations enable us to distinguish various stellar populations in SagDIG, as marked also by selected PARSEC evolutionary tracks overplotted in the figures. For the superposition of the evolutionary tracks, we adopt a distance modulus $(m - M)_0 = 25.06$ and an extinction of $A(\mathrm{F475W}) = 0.657$ mag, $A(\mathrm{F606W}) = 0.520$ mag and $A(\mathrm{F814W}) = 0.286$ mag. These values are discussed more extensively in Section 5. SagDIG is characterized by the presence of very old populations. RGB stars are indicatively marked by PARSEC evolutionary tracks of masses $M = 0.9$, 1.0 and 1.1 M$_{\odot}$ (cyan) while, for horizontal branch stars, we show two helium-burning tracks of $M = 0.85$ and 0.95 M$_{\odot}$ (pink). Because these are meant to be the most metal-poor stars in SagDIG, we have adopted a very low metallicity $Z = 0.0002$. The turn-off stars of these old populations are not visible in the CMDs of Fig. 1. Indeed, the deeper region of the observed main sequence (MS), around a magnitude of $m_{\rm F606W} \sim 27$, corresponds to the end of the H-burning phase of the track with $M \sim 1.5$ M$_{\odot}$, which is the faintest track plotted in red. This track is just near the separation mass between low- and intermediate-mass stars (i.e. between those that undergo or escape the helium flash). The track of $M \sim 1.7$ M$_{\odot}$ already belongs to the intermediate-mass progeny and shows a well-developed red clump. For all the tracks with mass $M \geq 1.5$ M$_{\odot}$, we use a larger metallicity, $Z = 0.0005$, as discussed below. We also note the presence of asymptotic giant branch (AGB) stars in the continuation of the RGB tracks above the corresponding RGB tips, and few of these are likely to correspond to intermediate-mass stars. The AGB population is not modelled in our simulations because the majority of it comes from older stellar populations.

Starting from the red clump, we can see the locus of the blue He-burning (BHeB) intermediate- and high-mass stars, which is clearly separated from the H-burning MS. This locus is marked by the blue loops of the other tracks plotted in the figure, which have initial masses of $M = 2.3$, 3.0, 4.0, 5.0, 8.0 and 12.0 M$_{\odot}$. We note that the upper MSs in the SagDIG CMDs seem to extend beyond that of the model of $M = 12$ M$_{\odot}$ and, for this reason, we also plot the tracks with $M = 16.0$ and 20.0 M$_{\odot}$. However, these tracks ignite He in the blue side of the CMDs and do not perform blue loops which appear in the tracks of less massive stars.

The clear separation of MS and BHeB stars makes the CMD of this galaxy, especially the $m_{\rm F606W}$ versus $(m_{\rm F606W} - m_{\rm F814W})$ CMD where the separation is striking, a powerful workbench for stellar evolution models at low metallicity.

2.2 Metallicity of SagDIG

From the colour of the RGB, Karachentsev, Aparicio & Makarova (1999) estimated the metallicity of SagDIG $[\mathrm{Fe/H}] = -2.45 \pm 0.25$, while Lee & Kim (2000) derived [Fe/H] in the range from −2.8 to −2.4. By comparing the colour differences between the RGB stars in the SagDIG and Galactic globular clusters (GGCs) fiducial lines, Momany et al. (2002) yielded a mean metallicity $[\mathrm{Fe/H}] = -2.1 \pm 0.2$ for the red giants, and Momany et al. (2005)

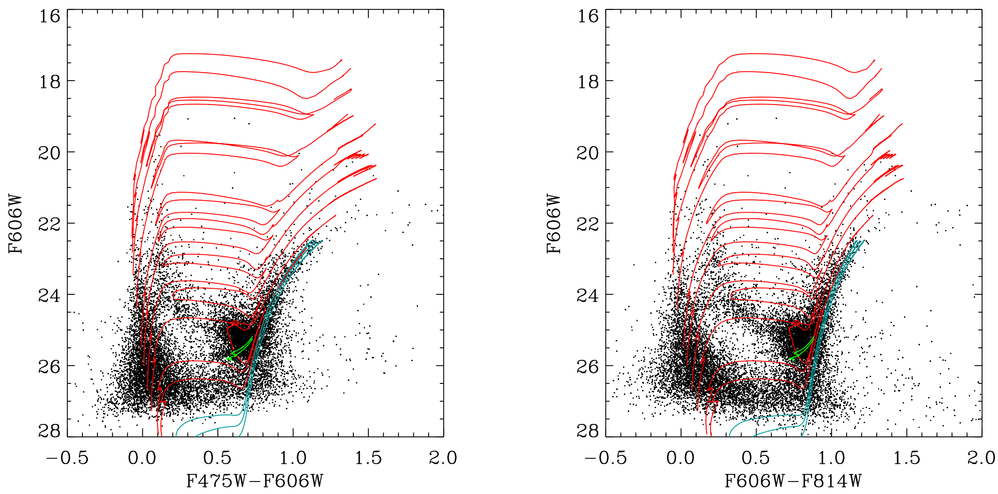

Figure 1. Observed colour–magnitude diagrams of SagDIG and evolutionary tracks computed by PARSEC V1.2 with EO = $0.7H_{\rm P}$. Cyan lines are tracks of $M = 0.9$, 1.0 and 1.1 $M_{\odot}$ with $Z = 0.0002$, marking the RGB stars. Green lines mark the horizontal branch evolutionary phases of stars with $M = 0.85$ and 0.95 $M_{\odot}$ and with $Z = 0.0002$. Red lines are tracks of $M = 1.5$, 1.7, 2.3, 3.0, 4.0, 5.0, 8.0, 12.0, 16.0 and 20.0 $M_{\odot}$ with $Z = 0.0005$.

gave the range [Fe/H] = −2.2 to −1.9 depending on different assumed reddening.

However, by analysing optical spectrophotometry of H II regions in SagDIG, Skillman, Terlevich & Melnick (1989) derived an oxygen abundance of 12+log(O/H) = 7.42, which is in accordance with the measurement of Saviane et al. (2002) who estimated the O abundance in the range 12+log(O/H) = 7.26–7.50. From the latter values, using for the Sun 12+log10(O/H) = 8.83 and $Z = 0.017$ (Grevesse & Sauval 1998), we obtain Z between 4.5×10^{-4} and 7.9×10^{-4}. If instead we use the solar values 12+log10(O/H) = 8.69 and $Z = 0.0134$ (Asplund et al. 2009), we obtain Z between 5.0×10^{-4} and 8.7×10^{-4}. We thus adopt for the young population of SagDIG a metallicity $Z = 5 \times 10^{-4}$, which is the lower value compatible with spectroscopic observations. We note that for the most recent populations Momany et al. (2005) infer a metallicity between $Z = 0.0001$ and 0.0004, by fitting the extension of the blue loops of intermediate- and high-mass stars using the previous Padova isochrones.

3 MODELS

Not only is there a clear separation between the H-burning MS and the BHeB stars in the CMDs of Fig. 1, but also red He-burning giants/supergiants (RSGs) can be fairly well separated from the older red giant stars. This allows us to test different prescriptions used in building models of intermediate- and high-mass stars, in particular those that are known to affect the extension and duration of the blue loops. We have already performed a similar analysis on three well-studied dwarf irregular galaxies (DIGs), Sextans A, WLM and NGC 6822, which are used to constrain the models at metallicities higher ($Z = 0.001$–0.004) than the one suitable for SagDIG ($Z = 0.0005$; Tang et al. 2014). The result of this analysis indicated that, if one keeps the extent of the core overshooting parameter fixed on the value resulting from comparison of low- and intermediate-mass stars (i.e. an overshooting length of about $0.25H_{\rm P}$ above the unstable core), then the blue loops of intermediate- and high-mass stars are significantly reduced with respect to the models computed without core overshooting. To restore the extent of the blue loops, significant overshooting at the base of the convective envelope is required, with a typical extent of a few $H_{\rm P}$. It is worth noting that any mechanism that increases the size of the fully He-exhausted region tend to shorten or even suppress the blue loops. This is also the case of models with rotational enhanced central mixing. In some cases, even models computed with the usual instability criterion and without any extended mixing face the problem of lacking extended blue loops, especially at high metallicities. The goal of this paper is to test if the conclusion obtained by Tang et al. (2014) remains valid also at very low metallicities. For this purpose, we model the brightest area of the CMD, which can be reasonably well represented by the last episode of star formation in SagDIG. We thus focus on stars brighter than $m_{\rm F606W} = 24$, where the completeness is 100, 99.7 and 98.8 per cent in F475W, F606W and F814W, respectively. This corresponds to a mass limit of ∼5.0 and ∼3.0 $M_{\odot}$ on the MS and on the He-burning phase respectively, as indicated in Figs 1 and 3.

3.1 Comparisons between the Schwarzschild criterion and the Ledoux criterion

Before embarking in this comparison, we stress that PARSEC models make use of the Schwarzschild criterion for convective instability. The boundary of the convective region can be determined by either the Schwarzschild criterion or the Ledoux criterion. According to Ledoux, the condition for the onset of convection is more restrictive than the Schwarzschild condition,

$$\nabla_{\rm rad} > \nabla_{\rm ad} + \nabla_{\mu}, \tag{1}$$

where $\nabla_{\rm rad}$, $\nabla_{\rm ad}$ and ∇_{μ} represent the radiative temperature gradient, adiabatic temperature gradient and molecular weight gradient, respectively. Here, ∇_{μ} can be expressed as

$$\nabla_{\mu} = -\left(\frac{\partial \ln \rho}{\partial \ln T}\right)^{-1}_{P,\mu} \left(\frac{\partial \ln \rho}{\partial \ln \mu}\right)_{P,T} \left(\frac{{\rm d} \ln \mu}{{\rm d} \ln P}\right). \tag{2}$$

In a region with homogeneous chemical composition, $\nabla_{\mu} = 0$, as expected, it becomes the Schwarzschild criterion:

$$\nabla_{\rm rad} > \nabla_{\rm ad}. \tag{3}$$

There have been claims in the literature that the use of the Ledoux criterion could eventually be more suitable in regions with variable mean molecular weight and it could give rise to more extended blue loops. This has been shown in the pioneering paper by Chiosi &

Summa (1970), who investigated the effect of the above two instability criteria on the morphology of the tracks and, specifically, on the extension of the blue loops. They found that the adoption of different criteria produces different sizes of semiconvective regions above the unstable core, and that only the model computed with the Ledoux criterion develops a blue loop. Notably, the model computed with the Schwarzschild criterion ignites central He at high effective temperature, before reaching the RSG phase, and only at the end of central He burning it slowly moves towards the latter phase. The different behaviour resulting from the adoption of different instability criteria can be understood by considering the competition between two important structural properties of the model, the relative size of the H-exhausted core and the mass pocket between the H-burning shell and the H–He discontinuity at the bottom of the convective envelope. As already shown in Lauterborn et al. (1971), because core overshooting during the H-burning phase has the effect of increasing the relative mass size of the H-exhausted core, it favours He ignition and burning in the red phase. However, it has been shown that the hydrostatic equilibrium location of He-burning models in the Hertzsprung–Russell diagram (HRD) is very sensitive to the mean molecular weight in the mass pocket between the H-exhausted core and the discontinuity in the H profile, left either by the development of intermediate convective regions and/or by the penetration of the convective envelope. Walmswell et al. (2015) have clearly shown that if the chemical composition of this mass pocket, which usually has an outward increasing H content, is artificially changed into a helium-rich mixture, the hydrostatic location of the model shifts to the blue region of the HRD.

This explains why the blue loop starts when the H-burning shell reaches the discontinuity of the mean molecular weight at the base of the H-rich envelope at an early phase during the central He burning (Tang et al. 2014). Three possibilities can arise, depending on when, eventually, the H-shell reaches the H-discontinuity after central H-exhaustion. If it happens very soon during its expansion phase before the star becomes a red giant, the path in the HRD is inverted and the star ignites and burns He as a blue supergiant. Only at central He exhaustion will the star move towards the red giant phase. This behaviour may be typical of most massive stars, especially at low metallicity. It corresponds to case B (model computed with the Schwarzschild criterion) in Chiosi & Summa (1970); this model does not perform a loop because it ignites He already in the blue loop hydrostatic configuration. The second case occurs when the H-shell reaches the discontinuity after He ignition in the red (super-)giant phase, but early enough during central He burning. In this case, the star performs a blue loop in the HRD as in case A (model computed with the Leodux criterion) of Chiosi & Summa (1970). Finally, if the H-shell reaches the discontinuity at a late time during central He burning, the star does not perform a blue loop and burns central He entirely as a red (super-)giant. However, this behaviour is not a general property of the adopted instability criterion. To demonstrate this, we show here two models with $M = 12\ \mathrm{M}_{\odot}$ computed with the two different instability criteria, and convective core overshooting is also considered in the models. As shown in the Kippenhahn diagrams of Fig. 2, the internal structure of the models is identical at the end of central H burning and both models are characterized by a rapid redward evolution followed by He ignition in the RSG phase, independently of the adopted instability criterion. The larger size of the H-exhausted core originated from the overshooting mixing forces both stars to ignite He in the supergiant phase. However, in the case of the Schwarzschild criterion (upper panel), a large intermediate convective region develops, shifting the location of the H–He discontinuity slightly deeper, as indicated by

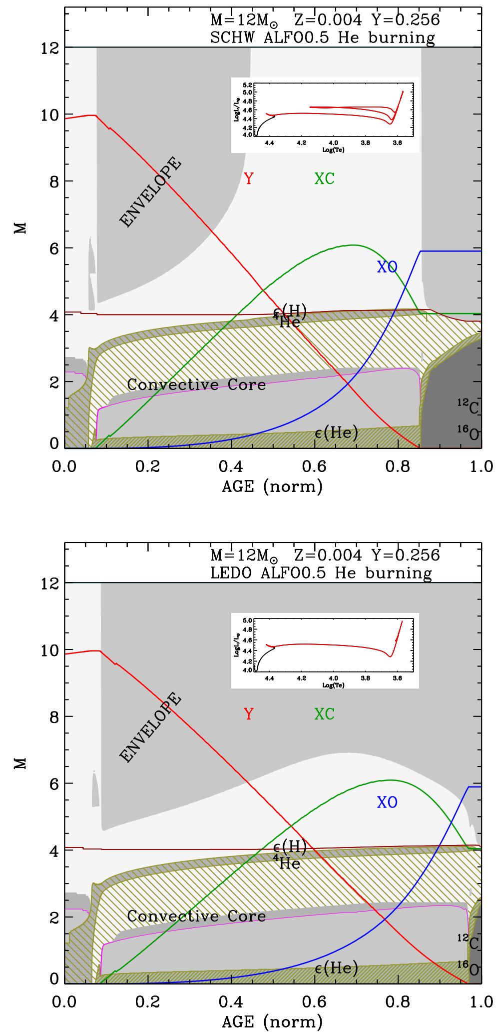

Figure 2. Kippenhahn diagrams of central He-burning stars of $M = 12\ \mathrm{M}_{\odot}$ and $Z = 0.004$ computed with different convection criteria: the Schwarzschild criterion (left panel) and the Ledoux criterion (right panel). The core overshooting parameter $\Lambda_c = 0.5$ is adopted. The brown line marks the location of the H–He discontinuity. The insets show the corresponding evolutionary tracks in the HRD.

the brown horizontal line, and effectively decreasing the size of the mass pocket between the H-exhausted core and the H–He discontinuity. Instead, using the Ledoux criterion (lower panel), which is more restrictive, the intermediate convective regions are smaller or even suppressed, and the resultant mass pocket is relatively larger. The difference with respect to the previous case is small, but in the former case, the H-burning shell is able to reach the discontinuity and a loop occurs, while in the latter case this occurs too late during He burning and the model does not perform a loop. Thus, the computations shown in Fig. 2 indicate that, in the presence of sizable convective overshooting during central H-burning, the model computed with the Schwarzschild instability criterion performs the blue loop while the model computed with the Ledoux criterion spends all the He-burning lifetime in the RSG phase. We thus illustrate that the effect found by Chiosi & Summa (1970) is not a general property of the instability criterion applied to massive stars. We instead confirm that the loop is activated if the H-shell reaches the H–He discontinuity during the early He-burning phase (Tang et al.

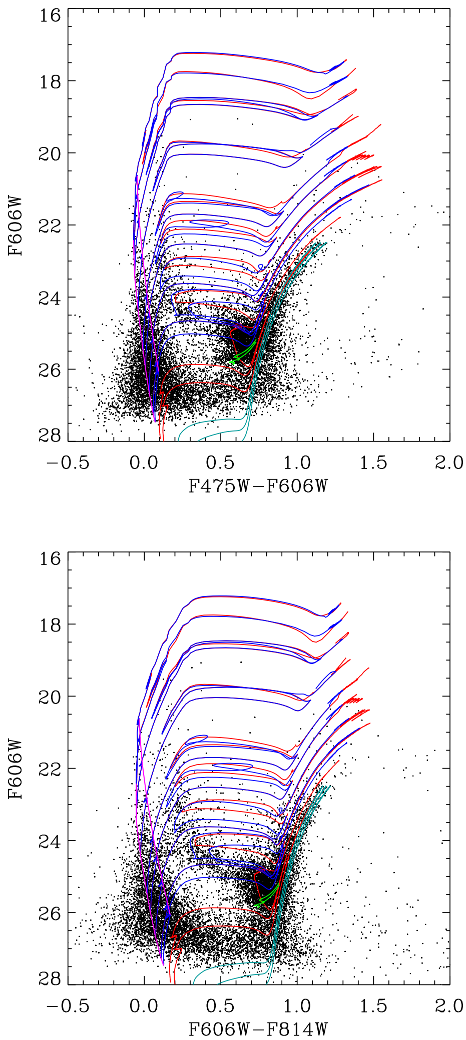

Figure 3. Observed CMDs of SagDIG and evolutionary tracks computed by PARSEC V1.2 with EO = $0.7H_{\rm P}$ (red) and 4 $H_{\rm P}$ (blue). Blue lines are tracks of $M = 2.1$, 2.3, 3.0, 4.0, 5.0, 8.0, 12.0, 16.0 and 20.0 $\mathrm{M}_{\odot}$ with $Z = 0.0005$. Pink lines mark the beginning and end of central H burning of stars with different initial masses, respectively.

2014). A possible explanation of why this effect triggers a blue loop has been advanced by Walmswell et al. (2015), who indicated that this is the hydrostatic equilibrium location of a class of central He-burning models with a fully discontinuous H profile.

3.2 Models with extended envelope overshooting

To conclude this section, we add to the CMDs of SagDIG in Fig. 3 the evolutionary tracks computed by assuming a large value of EO = $4H_{\rm P}$, which is the largest value adopted in Tang et al. (2014). These computations have been performed only for initial masses $M \geq 2.1$ $\mathrm{M}_{\odot}$ and the evolutionary tracks are shown in blue. The models run superimposed to the standard PARSEC models computed with EO = $0.7H_{\rm P}$ up to central He ignition. Then, models with larger EO ignite He at slightly lower luminosities (the red giant tips are fainter) and they burn central He at a significantly lower luminosity, both in the early red giant stage and in the blue loop phase. An interesting effect of a large EO is that, in the low mass range, the new models cross the Cepheid instability strip, being 0.5 mag fainter than the standard models. We also note that the blue loop is significantly more extended than that in standard models. These differences become smaller at increasing mass and practically disappear at masses $M \geq 8$ $\mathrm{M}_{\odot}$. As expected, the new models reproduce fairly well the region of the observed BHeB stars of SagDIG. We have also computed models with EO = $2H_{\rm P}$, which lie between the two extreme cases already discussed. In the next sections, we compare the simulated CMDs obtained by these models with the observed CMD.

4 SIMULATED COLOUR–MAGNITUDE DIAGRAMS

To construct a synthetic CMD of SagDIG, we follow the same procedure described in Tang et al. (2014), as briefly summarized below. For each of the three values of the EO parameter, EO = $0.7H_{\rm P}$, $2.0H_{\rm P}$ and $4.0H_{\rm P}$, we generate a large mock catalogue in the theoretical plane with the following steps.

(i) The star formation rate (SFR) ψ_m is specified as an exponential function of time, $\psi_m \propto \exp(t/\tau)$, where τ is an adjustable parameter and t is the stellar age, spanning from 1 Myr to 1 Gyr.

(ii) The age–metallicity relation (AMR) is replaced by a fixed value $Z = 0.0005$ as we have discussed in Section 2.2, because our analysis is limited to the youngest and brightest stars.

(iii) The initial mass function (IMF) ϕ_m is a broken power law in the form of $\phi_m \propto m^{-\alpha}$, where $\alpha = 0.4$ for $0.1 \leq m < 1$ $\mathrm{M}_{\odot}$, while the exponent is parametrized for $1\ \mathrm{M}_{\odot} \leq m \leq M_{\rm UP}$. The total mass is normalized to 1 in order to express SFR in units of $\mathrm{M}_{\odot}\ \mathrm{yr}^{-1}$.

(iv) The library of theoretical isochrones is computed by PARSEC, giving the luminosity L, the effective temperature $T_{\rm eff}$, the surface gravity g and other physical properties of stars as a function of stellar age t, initial mass $M_{\rm ini}$ and metallicity Z.

We transform the catalogue into the observational plane by means of bolometric corrections, as a function of $T_{\rm eff}$, g and Z, adopted from Marigo et al. (2008) and accounting for the distance. We finally add the effect of extinction and photometric errors. We can also include the effect of binarity, as discussed later. With the simulated catalogue that contains many more stars than the observed data, we perform 100 realizations of the CMD models to obtain, on one hand, the average and variance of the star luminosity function and, on the other hand, the best-fitting model to the observed luminosity function. We do not try more sophisticated statistical methods to reproduce the observed CMD, because our aim here is to obtain the best value of the EO parameter to be used with the fixed metallicity $Z = 0.0005$. Because we care about the extension of the blue loops in intermediate- and high-mass stars, we just select stars with mass $M \geq 1.9$ $\mathrm{M}_{\odot}$, and also set the apparent magnitude limit to $m_{\rm F606W} = 24$ in the simulation.

4.1 Simulated photometric errors

Momany et al. (2014) have estimated the photometric errors for observed stars in SagDIG from artificial star experiments. To account for photometric errors, we first bin their results in 0.1-mag steps as a function of the apparent magnitude in each filter, and calculate the median error for each bin. Then, we assign to each star in the mock catalogue an error that is randomly drawn from a Gaussian distribution with the standard deviation derived from the median corresponding to its magnitude (Tang et al. 2014). We note that because the observations are very deep, the simulated errors for stars brighter than 24 mag are small ($\lesssim$0.03 mag), as can be seen in Fig. 4.

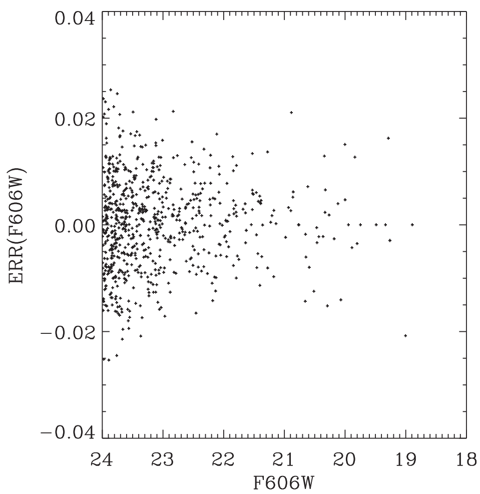

Figure 4. Simulated photometric errors as a function of the apparent magnitude in the F606W filter.

4.2 Foreground and internal extinction

Lee & Kim (2000) estimated a low foreground reddening $E(B-V) = 0.06$ based on the $(B-V)$ versus $(V-I)$ diagram, consistent with the value $E(B-V) = 0.07$ derived by Momany et al. (2002) from the $(V-I)$ colour distribution of foreground stars towards SagDIG, as the blue cut-off of the $(V-I)$ location is a function of reddening along the line of sight. Demers & Battinelli (2002) inferred $E(B-V) \approx 0.05$ in the same way, but using $(R-I)$ colour distribution. The infrared dust maps of Schlegel, Finkbeiner & Davis (1998) indicate a slightly higher reddening $E(B-V) = 0.12$. However, spectroscopic studies of the H II regions in SagDIG suggest a higher reddening. Skillman et al. (1989) calculated $c(H_\beta) = 0.33$ and $E(B-V) = 0.22$ is derived according to the relation $c(H_\beta) = 1.47E(B-V)$ (Seaton 1979). Saviane et al. (2002) obtained a similar value $E(B-V) = 0.19$ from the measurement of the Balmer decrement. As this method is based on the H line ratio, the estimated value includes both the foreground and the internal reddening. As young stars are physically associated with the warm interstellar medium (ISM), it is reasonable to believe they suffer higher reddening compared to old stars. This trend was also found in other DIGs (Bianchi et al. 2012; Tang et al. 2014). Bianchi et al. (2012) derived individual star-by-star extinction from their multiband data of Sextans A, WLM and NGC 6822 DIGs and this information was implemented in the synthetic CMD analysis by Tang et al. (2014). Because we lack multiband data for SagDIG and cannot repeat the same procedure with the same accuracy, we deal with the extinction in the following ways. The simplest way is to use a single value of the attenuation in each photometric band, as derived from the simultaneous alignment of the observed and modelled MS stars in both the $m_{\rm F606W}$ versus $(m_{\rm F475W} - m_{\rm F606W})$ and $m_{\rm F606W}$ versus $(m_{\rm F606W} - m_{\rm F814W})$ CMDs.

For the superposition of the evolutionary tracks, we adopt a distance modulus $(m-M)_0 = 25.06$ and an extinction of A(F475W) = 0.657 mag, A(F606W) = 0.520 mag and A(F814W) = 0.286 mag. These values are discussed more extensively in the following section.

5 RESULTS

The synthetic $m_{\rm F606W}$ versus $(m_{\rm F606W} - m_{\rm F814W})$ CMDs of SagDIG obtained with the three different values of EO are shown in Fig. 5. The observed CMD is represented by black points, while the best simulation is shown in green. The simulation refers to stars brighter than $m_{\rm F606W} = 24$. For ease of comparison, we draw the observed fiducial MS, which is indicated by the almost vertical black line at $(m_{\rm F606W} - m_{\rm F814W}) \sim 0$. It has been obtained by considering the median of the colours of MS stars, defined as stars bluer than $(m_{\rm F606W} - m_{\rm F814W}) = (m_{\rm F606W} - 18)/65$, in magnitude bins of $\Delta m_{\rm F606W} = 0.5$ in the range $21 \le m_{\rm F606W} \le 24$. The horizontal bar represents the standard deviation for the corresponding magnitude bin. It is calculated as the median absolute deviation, which is defined as the median of an array of differences between the colours of stars and the median colour. The fiducial MS locus derived from the best-fitting CMD is shown in red. Because the evolution up to central H exhaustion is not affected by EO, the MS loci are the same in the three simulated CMDs. The superposition of the observed and simulated MS loci has been obtained by assuming a single value of extinction for all stars in each of the three different photometric bands, A(F475W) = 0.657 mag, A(F606W) = 0.520 mag and A(F814W) = 0.286 mag. The adopted distance modulus is $(m-M)_0 = 25.06$. These values of extinction and distance modulus have also been used to draw the evolutionary tracks on the CMDs in Figs 1 and 3. Adopting $A_{\rm F606W}/A_V = 0.91$ (as in the Galactic extinction law with $R_v = 3.1$), we obtain $A_V = 0.57$. We compare the quantities $A_{\rm F475W}/A_V$ and $A_{\rm F814W}/A_V$ with those corresponding to other typical extinction laws in Fig. 6. We see that the value of $A_{\rm F475W}/A_V$ lies on the Calzetti extinction curve (Calzetti, Kinney & Storchi-Bergmann 1994), while the one of $A_{\rm F814W}/A_V$ falls slightly below the Galactic one (Cardelli, Clayton & Mathis 1989). The models shown in Fig. 5 correspond to the best fit selected from 100 stochastic realizations made with the same parameters, based on the merit function that measures the agreement between the observed and modelled luminosity functions of stars, both in the MS and in the blue-loop evolutionary phase. We notice that very bright stars ($m_{\rm F606W} \le 20$) in models are always much fewer than the observations. The parameters of the SFR and IMF adopted in the models are listed in Table 1.

The synthetic CMDs reproduce fairly well the main features of the observed CMD, except for the RGB. This is because we focus on newly formed stars, and exclude stars redder than the line $(m_{\rm F606W} - m_{\rm F814W}) = (29.95 - m_{\rm F606W})/7$, which, as shown in Figs 1 and 3, correspond to the RGB of the old populations. We note, however, that the simulated green-dot sequence in the case with EO = 0.7, representing red giant stars of the intermediate age populations, seems to be more populous than the corresponding data, while the discrepancy becomes smaller at increasing values of EO.

As discussed in Tang et al. (2014), models with enhanced EO produce more extended blue loops, which is also shown in Fig. 3. However, the simulations show two other interesting properties. One is that, at increasing EO, the relative fraction of BHeB stars increases while that of red He-burning stars decreases, explaining the better agreement between the simulated and observed red giants obtained with EO = 4. The other is that the population of yellow He-burning stars, say those with $0.4 \le (m_{\rm F606W} - m_{\rm F814W}) \le 0.7$, decreases at increasing EO. This is particularly evident in the magnitude range $23 \le m_{\rm F606W} \le 24$.

The effect of EO on the extension of the blue loops can be appreciated already by eye from Fig. 5, but in order to render it more clear, we derive the BHeB stars' main locus by using the same method adopted for the MS locus. The bins are the same used for the MS stars, though we recall that, at fixed initial mass, He-burning stars are brighter than H-burning stars. In

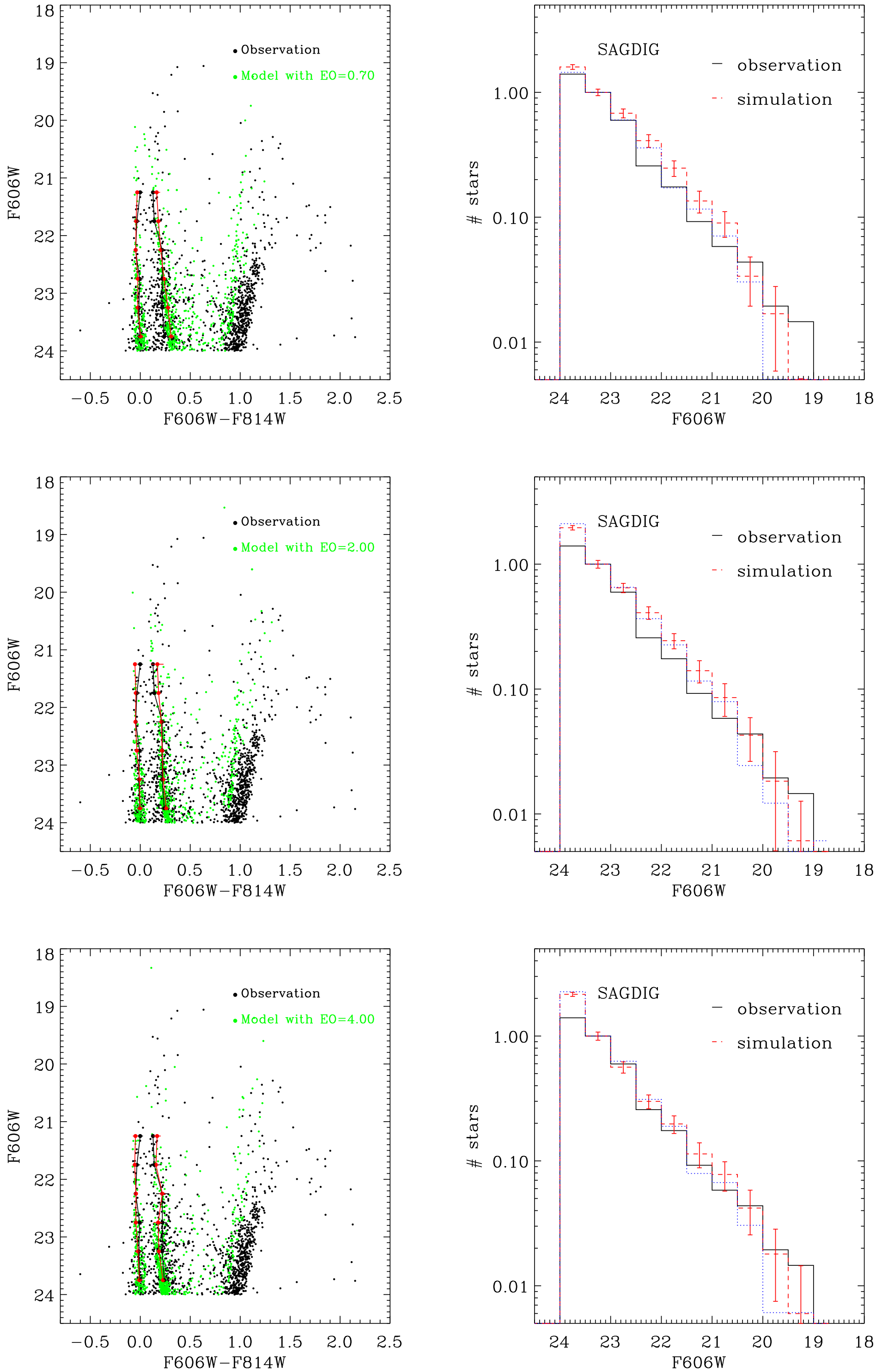

Figure 5. Left panels: comparisons of observed and modelled CMDs, EO = $0.7H_P$, EO = $2H_P$ and EO = $4H_P$, from top to bottom, respectively. The observation and simulation are represented by black and green points, and the corresponding medians and fiducial lines are marked in black and red, respectively. The error bars are calculated as the median absolute deviation. Right panels: the observed (black solid) and average simulated (red dashed) luminosity functions (LFs) with vertical standard deviation bars obtained from 100 simulations with fixed parameters. Blue dotted lines indicate the LFs of the best-fitting models.

order to derive the median colour, we have considered all stars redder than $(m_{F606W} - m_{F814W}) = (m_{F606W} - 18)/65$ and bluer than $(m_{F606W} - m_{F814W}) = 0.4$. The meaning of the error bar is the same as the one obtained for MS stars. The median locus of the observed BHeB stars is drawn in black and it runs almost parallel to the MS locus, but about 0.25 mag redder. The locus of the synthetic BHeB stars is drawn in red. For EO = $0.7H_P$, it is 0.1 mag redder than the observed one at magnitudes $23 \le m_{F606W} \le 24$. At brighter

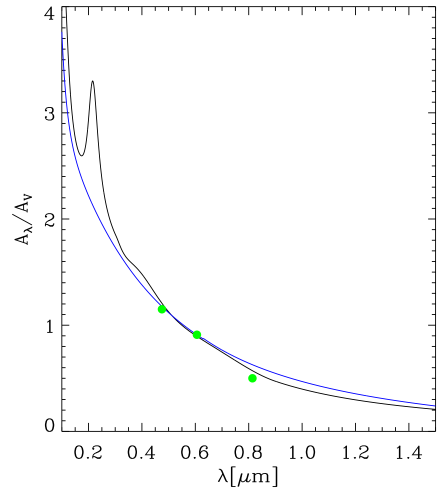

Figure 6. The reddening curve A_λ/A_V is shown as a function of λ. Our values A_λ/A_V for different photometric bands are shown by green solid dots. The black and blue lines represent the Galactic extinction law (Cardelli et al. 1989) and the Calzetti law (Calzetti et al. 1994), respectively.

Table 1. Parameters of the CMD simulations of SagDIG. ⟨SFR⟩ is the average SFR in the last 100 Myr.

EO	τ (yr)	α	SFR_0 ($M_\odot$ yr^{-1})	⟨SFR⟩ ($M_\odot$ yr^{-1})	M_{max} ($M_\odot$)	M_{bright} ($M_\odot$)
0.7	-2×10^9	2.05	8.79×10^{-4}	8.57×10^{-4}	39	11
2	-2×10^9	2.25	9.65×10^{-4}	9.41×10^{-4}	62	13
4	-2×10^9	2.15	1.18×10^{-3}	1.15×10^{-3}	30	30

magnitudes, the difference disappears. The locus of the models with EO = $2H_P$ runs superimposed to that of the observed data, in the magnitude range $23 \leq m_{F606W} \leq 24$, while using the models with EO = $4H_P$, it is slightly bluer than the observed one, in the same magnitude range $23 \leq m_{F606W} \leq 24$. We note that the difference between the observed and modelled BHeB loci is not large, even in the case of EO = $0.7H_P$. Actually, in the latter case, the largest difference is comparable to the standard deviations of the loci themselves. However, if we base our judgement more on the systematics of the effect than on its entity, it is clear that only models with larger EO are able to reproduce the extension of the blue loops in the magnitude range $23 \leq m_{F606W} \leq 24$.

5.1 Star formation rate

As in Tang et al. (2014), the SFR is represented by an exponential parametrization

$$SFR(t) = SFR_0 \times \exp\left(\frac{t}{\tau}\right), \tag{4}$$

where t represents the stellar age, SFR_0 is the current value of the SFR and τ is the characteristic e-folding time. The results are shown in Table 1. We find that the SFR in SagDIG increases towards recent times ($\tau < 0$). Considering the case of EO = $2H_P$, the average SFR in the last 100 Myr ($\sim 9 \times 10^{-4}$ $M_\odot$ yr^{-1}) is significantly lower than that we obtained for Sextans A (⟨SFR⟩ = 2.9×10^{-3} $M_\odot$ yr^{-1}), WLM (⟨SFR⟩ = 2.7×10^{-3} $M_\odot$ yr^{-1}) and NGC 6822 (⟨SFR⟩ = 3.7×10^{-3} $M_\odot$ yr^{-1}). It is worth noting that this average SFR is for the whole galaxy, while in those three galaxies the derived SFRs refer to selected star-forming regions. We also notice that the SFR does not change much for models with different EO, but in the case with high EO = $4H_P$, the SFR turns out to be ∼30 per cent larger than that in the case of EO = $0.7H_P$. Correspondingly, the mass formed in the recent burst amount to $M^* = 9.26 \times 10^5$ $M_\odot$ with EO = $4H_P$, while it is relatively smaller in the other two cases, $M^* \sim 7 \times 10^5$ $M_\odot$. Our value is close to that of Karachentsev et al. (1999) who found ⟨SFR⟩ = $6.6 \pm 0.8 \times 10^{-4}$ $M_\odot$ yr^{-1} in the age range 0.05–0.2 Gyr. Indeed, in the same period, we find ⟨SFR⟩ = 8.2×10^{-4} $M_\odot$ yr^{-1} using models with EO = $0.7H_P$. In Table 1, we also show the masses of the most massive and of the brightest stars found in the simulations.

5.2 Effects of differential extinction and binary stars

A remarkable property of the CMDs shown in Fig. 5 is that the standard deviations of the observed fiducial sequences are larger than the modelled ones. This indicates that both the observed MS and the observed BHeB sequence are more dispersed than predicted by the models, at least for stars brighter than $m_{F606W} = 24$. This cannot be ascribed to photometric errors because, besides being explicitly included in the simulation, they are, by far, too small to explain the effect. Thus, other explanations have to be found.

In the case of the MS, the discrepancy could be due to the well-known MS widening effect (i.e. the termination point of the observed MS is cooler than that predicted by the models). This could be appreciated in the comparison between the observed CMD and the evolutionary tracks in Fig. 3 where the width of the MS is marked by the pink lines. This discrepancy is one of the motivations that inspire the presence of extended mixing effects during the central H-burning phase of intermediate- and high-mass stars (Massevitch et al. 1979; Bressan et al. 1981). In the case of BHeB stars, the problem does not have a similar explanation. The star number counts in the evolved phases are proportional to the evolutionary lifetimes of the corresponding phases, and to explain a large dispersion one should invoke a mechanism that is able to slow down the transition from the RSG to the BSG phase, which is at present not known.

There are two other effects that could explain the widening of the sequences.

One is differential extinction. We have already mentioned that in previous analysis of DIGs, Bianchi et al. (2012) and Tang et al. (2014) have directly measured and then modelled differential extinction of individual stars. This effect certainly contributes to the widening of both the MS and the BHeB sequence and thus helps to fill the gap between them. Unfortunately, at variance with the quoted DIGs, in the case of SagDIG we lack the broad multiband photometry that allowed Bianchi et al. (2012) to obtain estimates of attenuation for individual stars. Nevertheless, we can try to estimate the size of this effect, by assuming that the models are correct. Applying the same method used in Tang et al. (2014), we derive a more realistic estimate of the extinction of individual stars, according to the trend of increasing attenuation at increasing luminosity, as shown in the diagram A(F606W) versus F606W of Fig. 7. Adopting the differential extinction, we obtain the simulated CMDs shown in Fig. 8. While the gap can be partly filled by introducing the differential reddening, it remains evident in the case of EO = $0.7H_P$. The gap decreases in the case of EO = $2H_P$ and almost disappears when a high EO is adopted, EO = $4H_P$. The fiducial lines of the MS and of the BHeB stars, drawn in the same way as in Fig. 5, show that the fact that the models with the standard value of EO = $0.7H_P$, are not able to reproduce the observed extended loops during the central He-burning phase, is not due to neglecting differential extinction. Even with differential extinction, a large value of EO ∼ 2.0 is favoured.

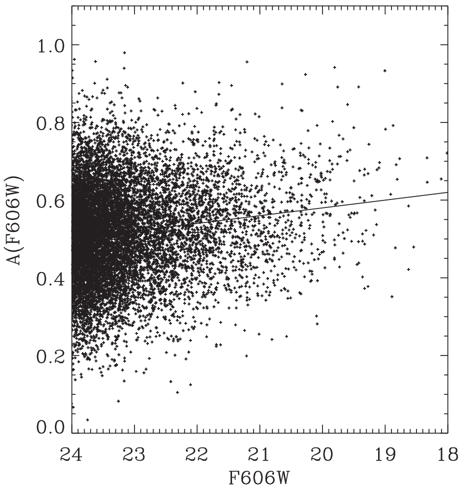

Figure 7. Differential extinction is assumed as a certain dispersion around a mean value $A(\mathrm{F606W}) = -0.02 \times m_{\mathrm{F606W}} + 0.98$ (black line).

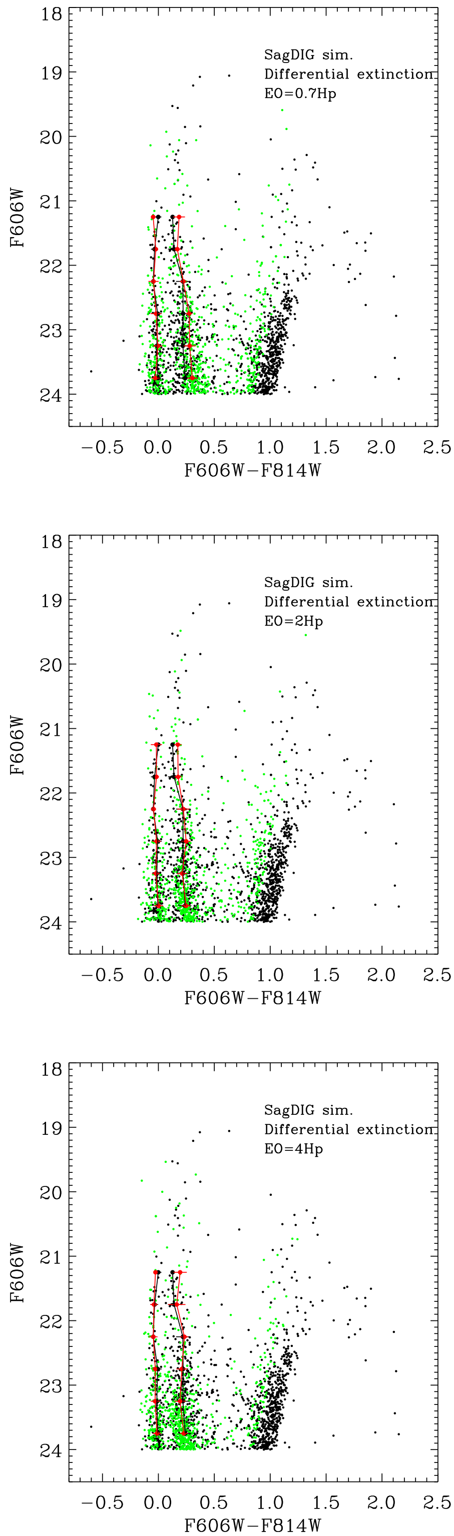

Figure 8. Best model obtained by PARSEC V1.2 with EO = $0.7H_\mathrm{P}$, $2H_\mathrm{P}$ and $4H_\mathrm{P}$ from top to bottom, respectively, with differential extinction.

Another effect that might contribute to widen the theoretical nominal sequences of single stars is the presence of binary stars. As is well known, the incidence of binarity in stars is high. Raghavan et al. (2010) analysed the sample of stars from the *Hipparcos* catalogue, suggesting that 33 per cent of solar-type stars in the solar neighbourhood are binaries. Moreover, young massive stars are believed more likely to be binaries. Sana, Gosset & Evans (2009) studied the optical spectra of O-type stars in NGC 6611 and derived the minimal binary fraction to be 0.44, but it could be increased up to 0.67 if all binary candidates are confirmed.

In order to estimate the effect of binaries on synthetic CMDs, we run a model with a percentage of binaries of 50 per cent. To reproduce the assumed 50 per cent contamination, we randomly combine the sample stars in the mock catalogue without assuming a particular value of the mass ratio, until we reach the total number of observed objects with the required binary fraction. Because, for binaries consisting of equal-mass components, the apparent magnitude can increase by up to 0.75 mag, to obtain a complete estimate of their effect above $m_{\mathrm{F606W}} = 24$, we first work on stars brighter than $m_{\mathrm{F606W}} = 25$. After taking into account the luminosity increase due to binarity, we further select objects brighter than $m_{\mathrm{F606W}} = 24$ and bluer than the line $(m_{\mathrm{F606W}} - m_{\mathrm{F814W}}) = (29.95 - m_{\mathrm{F606W}})/7$, as stars redder than this line are considered to be RGB stars. This procedure is repeated 100 times to obtain the best-fitting model, the average luminosity function and its standard deviation at the selected magnitude bins. In this case, we adopt a fixed extinction, as discussed in the previous section. Fig. 9 shows the simulated CMD obtained by the models with EO = $2H_\mathrm{P}$ and a binary fraction of 50 per cent. The inset shows the distribution of the mass ratios $q = M_2/M_1$ between the primary and secondary components, which is consistent with a flat distribution (Mermilliod et al. 1992).

Compared to the middle panel of Fig. 5, we see that the effect of binaries is to broaden the MS and also the BHeB sequence. The number of stars falling between these two sequences is larger than that in the case computed without considering binaries. However, the BHeB sequence is clearly split into two parallel sequences between $23 \le m_{\mathrm{F606W}} \le 24$, and the red He-burning sequence seems also too broad, as some of these stars move to the location of yellow giant/supergiant. In particular, the splitting of the BHeB sequence is not seen in the observed diagram, perhaps indicating that either the assumed binary fraction or the resulting mass ratio are too high for this galaxy of low metallicity. Furthermore, because of the asymmetric behaviour of the superposition of star pairs in the CMD, the fiducial lines shift towards the red side and, in order to reconcile the model with the observations, one should make use of a lower attenuation, by a factor $\delta(m_{\mathrm{F606W}} - m_{\mathrm{F814W}}) \sim 0.02$.

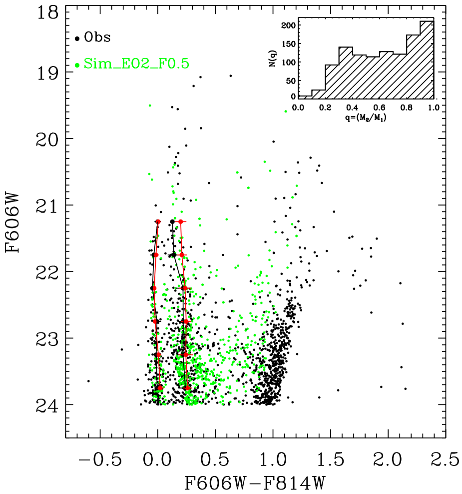

Figure 9. Best model obtained by PARSEC V1.2 with EO = $2H_{\rm P}$ and binary fraction $F = 0.5$. The insert shows the mass ratio distribution of binaries.

6 DISCUSSION AND CONCLUSION

In Tang et al. (2014), we had obtained strong indications that, in the presence of sizable overshooting from the convective core during central H burning, the standard PARSEC models with EO = $0.7H_{\rm P}$ fail to reproduce the width of the observed blue loops of intermediate- and high-mass stars in three star-forming dwarf galaxies in the Local Group (i.e. Sextans A, WLM and NGC 6822), characterized by low metallicity, $0.001 \le Z \le 0.004$. Meanwhile, we found that a significant EO at the bottom of the convective envelope, EO = 2.0–$4.0H_{\rm P}$, must be used to overcome this discrepancy in models with metallicity typical of the aforementioned galaxies, $0.001 \le Z \le 0.004$. We stressed that this discrepancy could be cured by adopting a metallicity significantly lower than the observed one, which however indicates that using the extension of the blue loops predicted by models to infer the metallicity of the galaxies could be risky. In this paper, we continue this investigation by considering the case of SagDIG, a nearby star-forming DIG whose metallicity is estimated to be even lower than that of the aforementioned galaxies, $Z = 0.0005$. This galaxy is an ideal workbench to test the performance of models of intermediate- and high-mass stars because it harbours a recent burst of star formation, and it is sufficiently nearby that intermediate-mass stars with masses as low as $M = 2$ M$_{\odot}$ can be detected. The foreground contamination has been eliminated using proper motions of individual stars (Momany et al. 2014).

From a preliminary superposition of the standard PARSEC evolutionary tracks with EO = $0.7H_{\rm P}$ and the observed CMD of SagDIG, we already see that the models are not able to reproduce the observed loops. This has already been noticed by Momany et al. (2005) who, in an attempt to determine the metallicity of the galaxy from the blue-loop superposition, were forced to try also the lowest value of metallicity of the old Padova models, $Z = 0.0001$.

Before performing new calculations with enhanced EO, as suggested by Tang et al. (2014), we discuss whether the problem could be alleviated by adopting the Ledoux criterion instead of the Schwarzschild criterion for the determination of the unstable region. On one hand, it has already been shown in the past that the adoption of the Ledoux criterion may favour the development of extended blue loops (Chiosi & Summa 1970). On the other hand, the fact that the problem of short blue loops is found even in the tracks of intermediate-mass stars, for which the results should be independent of the adopted instability criterion because they do not possess intermediate unstable region (within the profile of chemical composition), suggests that the reason should be different. By analysing a model of $M = 12$ M$_{\odot}$ and $Z = 0.004$ under standard PARSEC assumptions, which evolves without performing a blue loop, we find that the Ledoux criterion tend to suppress the blue loop, in the sense that the star favours the redward evolution after central H burning. This is apparently in contrast to the results reported by Chiosi & Summa (1970), who indicated that the Ledoux criterion favours the blue loop. However, a thorough inspection of that influential paper shows that their model with the Schwarzschild criterion does not perform a blue loop only because it already begins central He burning in the blue-loop region (i.e. as a BHeB star). With a series of new models not reported here for conciseness, we show that at He ignition, the mass pocket between the H-exhausted core and the H/He discontinuity is already negligible, fully confirming the finding of Walmswell et al. (2015). The Schwarzschild criterion allows the formation of a larger intermediate convective shell than in the case of the Ledoux criterion, and this convective shell pushes the H/He discontinuity deeper in the star, reducing the above mass pocket. Thus, the case A model in Chiosi & Summa (1970) begins He burning already in the BHeB equilibrium configuration and not in the RSG stage, without the need of performing a blue loop. In contrast, their case B model, with the Ledoux criterion, encounters the condition of a thin mass pocket between the H-exhausted core and the H/He discontinuity, slightly later during the evolution, after He ignition in the RSG phase, and thus performs a blue loop. When significant core overshooting is allowed during the H-burning phase, the situation changes critically. With the H-exhausted core being larger than that in the case without core overshooting, its contraction after central H-burning is stronger, pushing the star into the RSG stage, independently of the adopted instability criterion. These are the two cases shown in Fig. 2 for $M = 12$ M$_{\odot}$ and $Z = 0.004$. However, although the differences between the models computed with the two different criteria are minimal, the track computed with the Schwarzschild criterion develops a larger intermediate convective region that deepens slightly the H–He discontinuity than in the one computed with the Ledoux criterion. The former develops the blue loop while, in the latter case, the condition of a thin intermediate layer is encountered only towards the end of central He burning, when the BHeB structure is no longer a possible configuration for the star so that it burns the entire central He in the RSG stage.

Having definitely excluded the Ledoux criterion as a possible cure of the problem of the loop extension, we computed additional evolutionary tracks with larger values of EO = $2H_{\rm P}$ and EO = $4H_{\rm P}$. Combining the results with other specified parameters, the IMF and SFR law, the photometric errors and the extinction in our own CMD simulator, we construct the synthetic CMDs that are compared with the observed one of SagDIG. In all models, the location of the observed fiducial MS is well reproduced with a reasonable value of the attenuation. This is expected as the MS phase is not affected by EO and the match is actually used to determine the extinction to be adopted in the simulated CMDs. As expected, models with larger EO perform more extended blue loops, and their BHeBS get closer to the MS. In order to decide which value of EO reproduces better the observed extension of the blue loops, we also draw and compare the fiducial lines corresponding to the BHeBS of the synthetic and of the observed CMDs. We find that the model with EO = $2H_{\rm P}$ matches the observations best, while the blue loops predicted by the case EO = $0.7H_{\rm P}$ are not hot enough and those predicted in the case of EO = $4H_{\rm P}$ are likely hotter than the data indicate.

It is worth stressing that, because the value of the EO is not an adjustable parameter in the CMD comparison, we have a no better and more statistically sound method to decide which is the best case, than that of comparing the fiducial MSs. We have also tested how the results depend on other additional assumptions concerning the attenuation and the possible effect of binarity. If we assume a differential attenuation with a reasonable model (Fig. 7) where the attenuation has a certain dispersion around a mean value that increases with the intrinsic luminosity of the stars (Tang et al. 2014), the overall CMD fit looks better but the preferred value of the EO remains unchanged. However, because of the dispersion introduced in the synthetic CMD, the uncertainty of the fiducial points (the horizontal bars in the CMD figures), corresponding to the colour median absolute deviation in each magnitude bin, becomes slightly larger. To single out the effect of binarity, we consider the case with constant attenuation and a binary fraction of 50 per cent. The effect of binaries is to broaden both the MS and the BHeB sequence, with the consequence that the number of stars falling between the two sequences is larger than that in the case computed without considering binaries. However, the BHeB sequence is clearly split into two parallel sequences between $23 \le m_{\mathrm{F606W}} \le 24$, and the red He-burning sequence becomes less populated, as some of these stars move into the region populated by yellow giants/supergiants. The splitting of the BHeB sequence is not seen in the observed diagram, perhaps indicating that either the assumed binary fraction or the resulting mass ratio are too high for this galaxy of low metallicity. Furthermore, because of the asymmetric behaviour of the superposition of star pairs in the CMD, the fiducial lines shift towards the red side and, in order to reconcile the model with the observations, one should adopt a slightly lower attenuation, $\delta(m_{\mathrm{F606W}} - m_{\mathrm{F814W}}) \sim 0.02$. Even in this case, the models that perform better are those computed with EO $= 2H_{\mathrm{P}}$.

The results of this paper are consistent with those found by Tang et al. (2014) for three galaxies with slightly higher metallicities than the one considered here. Thus, the current investigation corroborates the finding that the mixing scale below the formal Schwarzschild border in the envelopes of intermediate- and high-mass stars must be significantly higher than currently assumed in PARSEC models. We recall that there are other conditions where strong mixing below the conventional instability region is invoked, such as, for example, to enhance the efficiency of the carbon dredge-up during the thermally pulsing AGB phase (Kamath, Karakas & Wood 2012). However, we note that such a high value is likely to be incompatible with the location of the RGB bumps observed in globular clusters, which can be well reproduced by the models using an EO no larger than EO $= 0.5H_{\mathrm{P}}$. Thus, if the interpretation in terms of mixing into the stable regions due to convection is correct, it is likely that the mixing scale below the formal Schwarzschild border is not a fixed fraction of the pressure scaleheight, as assumed in usual extensions of the MLT, but instead it depends on the interior structure of the star. In fact, our results highlight a difficulty inherent in the MLT, which, by itself, cannot predict the size of the velocity field. In this respect, it is interesting to compare our finding with the results of a recent three-dimensional implicit large eddy simulation of the turbulent convection in the envelope of a 5-$\mathrm{M}_{\odot}$ red giant star (Viallet et al. 2013). The simulation refers to the envelope of a 5-$\mathrm{M}_{\odot}$ star at the end of central He burning. The convective unstable region extends inward from an outer radius $R \sim 4.1 \times 10^{12}$ cm to an inner radius $R \sim 2.2 \times 10^{12}$ cm, where the Schwarzschild condition of stability is satisfied ($\nabla_{\mathrm{rad}} = \nabla_{\mathrm{ad}}$; see their fig. 17). At this layer, the velocity field shows a sudden drop, but does not vanish; it ceases to be dominated by the radial components and begins to be dominated by the transversal components (see their fig. 4). This indicates a clear regime of convective turn-over extending for about $0.6H_{\mathrm{P}}$ ($\sim 0.25 \times 10^{12}$ cm) below the formally unstable region, which the authors recognize as the lower boundary of the convective envelope. In this region, the rms velocities decrease from $\sim 10^5$ cm s^{-1} to $\sim 10^4$ cm s^{-1}. Thus, the simulation shows that there is a region of about $0.6H_{\mathrm{P}}$ below the formal Schwarzschild border where velocities remain significantly high, characterized by the transversal components being about twice the radial ones. From fig. 4 of Viallet et al. (2013), we can also see that the velocity field extends much below this point and, though it is difficult to evaluate from the figure alone, the rms velocities are clearly larger than $\sim 10^3$ cm s^{-1}, even at several $\sim 10^{11}$ cm below the Schwarzschild border.

In our track of $M = 5$ $\mathrm{M}_{\odot}$ and $Z = 0.004$, at the stage of maximum penetration near the tip of the first red giant ascent – not the second as in the Viallet et al. (2013) simulation – the model has the following structure. The stellar radius is $R \sim 7.4 \times 10^{12}$ cm and the inner Schwarzschild border is at $R \sim 0.8 \times 10^{12}$ cm. The size of the unstable region is $\sim 6.6 \times 10^{12}$ cm. The maximum velocities predicted using the MLT are a few $\sim 10^5$ cm s^{-1}, but drop to $\sim 2.4 \times 10^4$ cm s^{-1} near the Schwarzschild border. The pressure scaleheight at the inner Schwarzschild border is $H_{\mathrm{P}} \sim 4 \times 10^{11}$ cm and a mixing scale of $0.7H_{\mathrm{P}}$ corresponds to $\delta_r(0.7) \sim 2.4 \times 10^{11}$ cm, while that of $4H_{\mathrm{P}}$ corresponds to $\delta_r(4) \sim 6 \times 10^{11}$ cm. This non-linearity is due to the fact that we measure the overshooting region in terms of pressure and not in length, and that the pressure scaleheight below the bottom of the convective region decreases at decreasing radius (while it keeps increasing again in the inner He core). Our convective region is thus not very different from the one described in the Viallet et al. (2013) simulation. With radial velocities of about $\sim 10^3$ cm s^{-1}, convection can span a distance of $\delta_r(4)$ in about 20 yr, which, because our model spends a few thousand years before convection begins to retreat, is about 100 times shorter than the evolutionary time of the star in this phase. Thus, at first glance, the Viallet et al. (2013) simulation indicates that the internal mixing of about 2–$4H_{\mathrm{P}}$ below the formal convective border is possible in an evolutionary time-scale. What we have neglected in this simple discussion are the effects of the molecular weight discontinuity that forms between the outer H-rich and the inner He-rich regions, which could strongly limit or even suppress the penetration of convective motions (e.g. Bressan et al. 1981). At face value, our finding indicates that turbulent entrainment into the stably stratified layers (Meakin & Arnett 2007) should be quite efficient in the envelopes of such stars. Clearly, detailed numerical simulations (e.g. Arnett et al. 2015), especially addressed to the analysis of the mixing efficiency in presence of chemical composition gradient, would be extremely helpful to clarify this issue.

ACKNOWLEDGEMENTS

We thank S. Charlot and Y. Chen for helpful discussions. AB acknowledges support from INAF through grant PRIN-2014-14. PM acknowledges support from *Progetto di Ateneo 2012*, University of Padova (ID: CPDA125588/12).

REFERENCES

Alongi M., Bertelli G., Bressan A., Chiosi C., 1991, A&A, 244, 95
Arnett W. D., Meakin C., Viallet M., Campbell S. W., Lattanzio J. C., Mocák M., 2015, ApJ, 809, 30
Asplund M., Grevesse N., Sauval A. J., Scott P., 2009, ARA&A, 47, 481
Bertelli G., Bressan A. G., Chiosi C., 1985, A&A, 150, 33

Bertelli G., Betto R., Chiosi C., Bressan A., Nasi E., 1990, A&AS, 85, 845
Bianchi L., Efremova B., Hodge P., Massey P., Olsen K. A. G., 2012, AJ, 143, 74
Böhm-Vitense E., 1958, ZAp, 46, 108
Bressan A. G., Chiosi C., Bertelli G., 1981, A&A, 102, 25
Bressan A., Marigo P., Girardi L., Salasnich B., Dal Cero C., Rubele S., Nanni A., 2012, MNRAS, 427, 127
Bressan A., Marigo P., Girardi L., Nanni A., Rubele S., 2013, European Physical Journal Web of Conferences, 43, 3001
Calzetti D., Kinney A. L., Storchi-Bergmann T., 1994, ApJ, 429, 582
Cardelli J. A., Clayton G. C., Mathis J. S., 1989, ApJ, 345, 245
Chen Y., Girardi L., Bressan A., Marigo P., Barbieri M., Kong X., 2014, MNRAS, 444, 2525
Chiosi C., Summa C., 1970, Ap&SS, 8, 478
Demers S., Battinelli P., 2002, AJ, 123, 238
Girardi L., Rubele S., Kerber L., 2009, MNRAS, 394, L74
Grevesse N., Sauval A. J., 1998, Space Sci. Rev., 85, 161
Kamath D., Karakas A. I., Wood P. R., 2012, ApJ, 746, 20
Karachentsev I., Aparicio A., Makarova L., 1999, A&A, 352, 363
Lauterborn D., Refsdal S., Weigert A., 1971, A&A, 10, 97
Lee M. G., Kim S. C., 2000, AJ, 119, 777
Marigo P., Girardi L., Bressan A., Groenewegen M. A. T., Silva L., Granato G. L., 2008, A&A, 482, 883
Massevitch A. G., Popova E. I., Tutukov A. V., Iungelson L. R., 1979, Ap&SS, 62, 451
Meakin C. A., Arnett D., 2007, ApJ, 667, 448
Mermilliod J.-C., Rosvick J. M., Duquennoy A., Mayor M., 1992, A&A, 265, 513
Momany Y., Held E. V., Saviane I., Rizzi L., 2002, A&A, 384, 393
Momany Y. et al., 2005, A&A, 439, 111
Momany Y. et al., 2014, A&A, 572, A42
Raghavan D. et al., 2010, ApJS, 190, 1
Robertson J. W., 1972, ApJ, 173, 631
Sana H., Gosset E., Evans C. J., 2009, MNRAS, 400, 1479
Saviane I., Rizzi L., Held E. V., Bresolin F., Momany Y., 2002, A&A, 390, 59
Schlegel D. J., Finkbeiner D. P., Davis M., 1998, ApJ, 500, 525
Seaton M. J., 1979, MNRAS, 187, 73P
Skillman E. D., Terlevich R., Melnick J., 1989, MNRAS, 240, 563
Stothers R. B., Chin C-W., 1991, ApJ, 374, 288
Tang J., Bressan A., Rosenfield P., Slemer A., Marigo P., Girardi L., Bianchi L., 2014, MNRAS, 445, 4287
Viallet M., Meakin C., Arnett D., Mocák M., 2013, ApJ, 769, 1
Walmswell J. J., Tout C. A., Eldridge J. J., 2015, MNRAS, 447, 2951

This paper has been typeset from a TEX/LATEX file prepared by the author.